Structural mechanisms of the high-pressure phase transitions in the elements of group IVa

2007 J. Phys.: Condens. Matter 19 275204

(http://iopscience.iop.org/0953-8984/19/27/275204)

IOP PUBLISHING JOURNAL OF PHYSICS: CONDENSED MATTER

J. Phys.: Condens. Matter **19** (2007) 275204 (19pp) doi:10.1088/0953-8984/19/27/275204

Structural mechanisms of the high-pressure phase transitions in the elements of group IVa

Hannelore Katzke[1] **and Pierre Tolédano**[2]

[1] Institute of Geosciences, Crystallography, University of Kiel, Olshausenstraße 40, 24098 Kiel, Germany
[2] Department of Physics, Faculty of Sciences, University of Picardie, 33 rue Saint-Leu, 80000 Amiens, France

E-mail: hanne@min.uni-kiel.de

Received 21 December 2006, in final form 15 March 2007
Published 1 June 2007
Online at stacks.iop.org/JPhysCM/19/275204

Abstract

Displacive mechanisms are proposed for the high-pressure structural transitions which take place in the elements of group IVa. The mechanisms are analysed in the framework of the Landau theory of phase transitions. In carbon the polymorphs are shown to correspond to limit states resulting from critical fractional displacements and critical strains, the corresponding order parameters being defined as periodic functions of the displacements. In Si, Ge, Sn and Pb a number of unifying features are discussed in connection with the electronic structures of these elements.

(Some figures in this article are in colour only in the electronic version)

1. Introduction

Because of their technological importance, the elements of group IVa have been extensively studied for many decades. However, it is only recently that the structures of most of their high-pressure phases have been elucidated [1–4]. Thus the sequences of structures occurring under pressure are now well identified up to 275 GPa in carbon, 248 GPa in silicon, 190 GPa in germanium, 120 GPa in tin, and 270 GPa in lead. Therefore, one can go beyond the theoretical considerations which have attempted to predict or justify the stability of new structures in these elements, and to search for a possible unifying scheme that would explain the similarities and differences which are found in their phase diagrams. Figure 1 summarizes the sequences of phases disclosed on increasing pressure in the elements of group IVa. One can see that the simplicity of the equilibrium phase diagram of carbon, which contains only two (graphite and diamond) phases, is in contrast with the rich polymorphism found in Si and Ge. These two elements display remarkably similar sequences of seven and six different structures, respectively. Their two lower-pressure structures are also found in tin but the higher-pressure structures of tin are different. The diamond-type structure is absent from lead, the phase

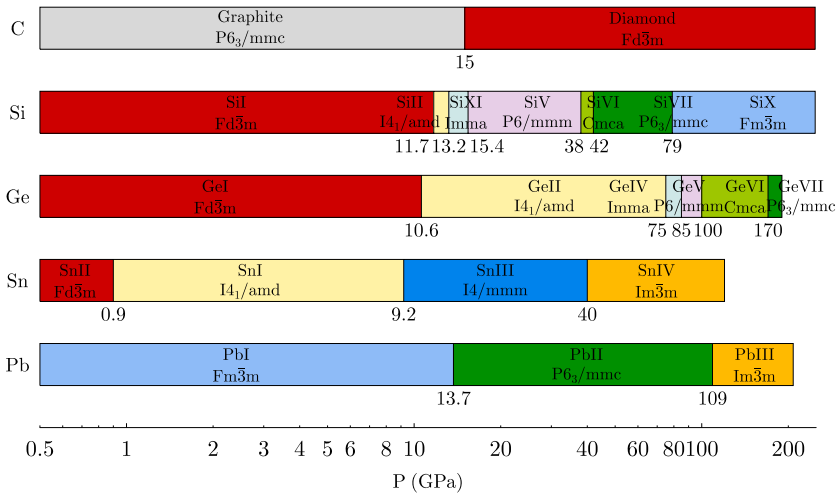

Figure 1. Symmetry of the phases taking place with increasing pressure in the elements of group IVa.

diagram of which seems to belong to another class, although it can be noted that its successive fcc, hcp and bcc structures coincide with the highest-pressure structures found, respectively, in Si, Ge and Sn.

In this article we propose in section 2 a comprehensive description of the displacive transition mechanisms taking place between the neighbouring structures of the elements of group IVa. Then, in section 3, a symmetry analysis of these mechanisms is performed, together with considerations on the evolution of the electronic structures of the elements with increasing pressure. It allows, to some extent, a more precise understanding of the diversity of phase diagrams found for the elements of this group, which is summarized in section 4.

2. Structural transition mechanisms

2.1. Carbon

The transformation mechanism from graphite to diamond is not yet fully understood. In particular, the role played in this mechanism by rhombohedral graphite [5] or hexagonal diamond is still questioned. The different theoretical models proposed for the graphite–diamond transition [6–12, 15] involve a hybridization change for the bonding electrons and structural mechanisms describing the conversion from one structure to the other in terms of reordering in the hexagonal layer stacking, supplemented by macroscopic strains. Here we show that the structural changes between carbon polymorphs can be described in a unified way as reconstructive transitions of the displacive type, the transitions occurring via a common substructure of monoclinic or orthorhombic symmetry. In this description the polymorphs appear as *limit states* resulting from definite critical displacements and critical strains.

Figure 2 represents the assumed displacive mechanisms transforming hexagonal graphite (HG), rhombohedral graphite (RG), hexagonal diamond (HD) and cubic diamond (CD) into each other. Figures 2(a), (c), (h) and (i) show that the carbon structures possess a common substructure displaying an orthorhombic $Cmcm$ (HG), $Bmmb$ (HD) or monoclinic $C2/m$ (RG, CD) symmetry, whose basic vectors ((**a**), (**b**), (**c**)) are related to the basic vectors of the

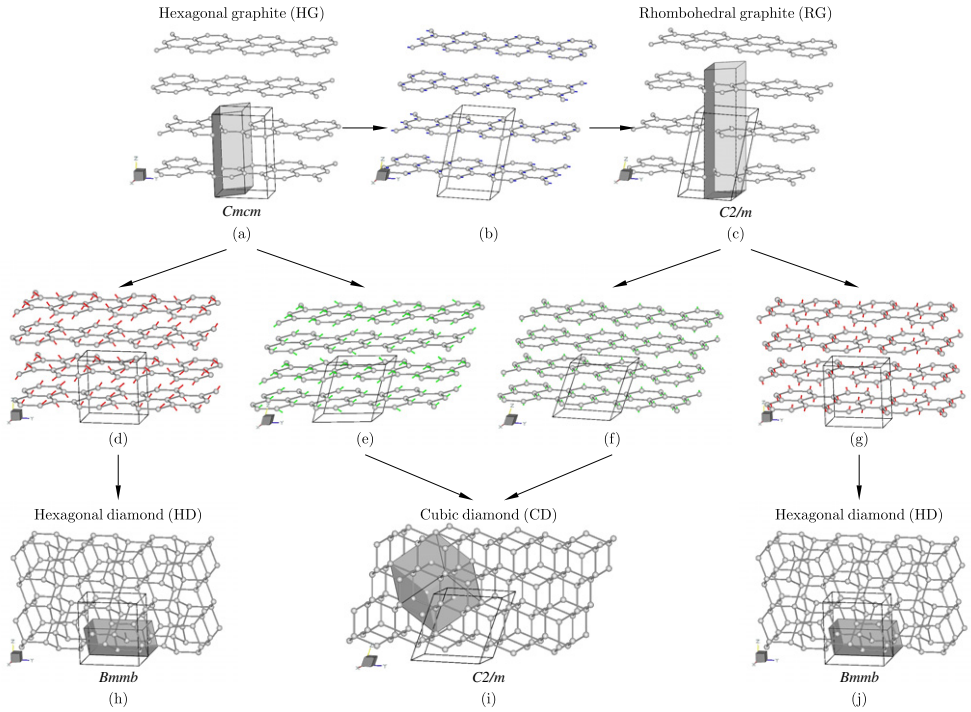

Figure 2. Structural mechanisms for the reconstructive phase transitions between carbon polymorphs via a common substructure: (1) HG → HD ((a) → (d) → (h)), (2) HG → CD ((a) → (e) → (i)), (3) HG → RG ((a) → (b) → (c)), (4) RG → CD ((c) → (f) → (i)) and (5) RG → HD ((c) → (g) → (j)). The conventional hexagonal (HG, RG and HD) and cubic (CD) unit cells are represented by grey polyhedra in (a), (c), (h), (j) and (i). The unit cells of their common substructures are shown in all figures by thin lines. The small arrows in (b), (d), (e), (f) and (g) represent the real magnitudes of the atomic displacements.

conventional hexagonal (HG, RG, HD) or cubic (CD) unit cells of the different allotropes by

$$\begin{aligned}
\mathbf{a} &= \mathbf{a}_{\mathrm{HG}} = \mathbf{a}_{\mathrm{RG}} = -\mathbf{a}_{\mathrm{HD}} = 1/2(\mathbf{a}+\mathbf{b})_{\mathrm{CD}} \\
\mathbf{b} &= (\mathbf{a}+2\mathbf{b})_{\mathrm{HG}} = (\mathbf{a}+2\mathbf{b})_{\mathrm{RG}} = \mathbf{c}_{\mathrm{HD}} = -1/2(\mathbf{a}+\mathbf{b}-2\mathbf{c})_{\mathrm{CD}} \\
\mathbf{c} &= \mathbf{c}_{\mathrm{HG}} = 1/3(\mathbf{a}+2\mathbf{b}+2\mathbf{c})_{\mathrm{RG}} = (\mathbf{a}+2\mathbf{b})_{\mathrm{HD}} = 1/2(\mathbf{a}+\mathbf{b}+2\mathbf{c})_{\mathrm{CD}}
\end{aligned} \tag{1}$$

in accordance with the observed orientational relations reported in [13] that $[001]_{\mathrm{HG}} \parallel [120]_{\mathrm{HD}}$, $[100]_{\mathrm{HG}} \parallel [100]_{\mathrm{HD}}$ and $[120]_{\mathrm{HG}} \parallel [001]_{\mathrm{HD}}$. The lattice parameters of the transformed unit cells are given in table 1. The atomic displacement field transforming HG into CD is shown in figures 2(a) → (d) → (h). It consists of antiparallel *fractional* displacements $\pm\frac{1}{16}\mathbf{b}$ and $\pm\frac{1}{12}\mathbf{c}$ combined with $\pm\frac{5}{48}\mathbf{b}$ and $\pm\frac{1}{12}\mathbf{c}$, the carbon atoms initially in 2b and 2c positions of $P6_3/mmc$ being shifted into positions 4f. The HG → HD transition involves a drastic compression of about 35% along **c** and small decompression (2%) and compression (6%) along **a** and **b** respectively.

A similar mechanism, represented in figures 2(a) → (e) → (i), holds for the HG → CD transition. Starting from the transformed unit cell of HG, the CD structure results from the reduction of the angle α from 90° in HG to 70.529° in CD, and a set of antiparallel fractional displacements $\pm\frac{1}{16}\mathbf{b}$ and $\pm\frac{1}{16}\mathbf{c}$, combined with $\pm\frac{5}{48}\mathbf{b}$ and $\pm\frac{1}{16}\mathbf{c}$. The CD unit cell, in which the carbon atoms occupy the 8a positions of space group $Fd\bar{3}m$, is deduced from the monoclinic

Table 1. Lattice parameters of the conventional unit cells and the common substructure calculated after equation (1) for the carbon polymorphs.

Polytype	a (Å)	b (Å)	c (Å)	α	γ	Space group
HG	2.464	2.464	6.708		120	$P6_3/mmc$
	2.464	4.268	6.708			$Cmcm$
RG	2.456	2.456	10.041		120	$R\bar{3}m$
	2.456	4.254	6.843	78.040		$C2/m$
HD	2.522	2.522	4.119		120	$P6_3/mmc$
	2.522	4.119	4.369			$Bmmb$
CD	3.567	3.567	3.567			$Fd\bar{3}m$
	2.522	4.368	4.368	70.529		$C2/m$

unit cell by shifting the origin by $p = \left(0, \frac{1}{16}, \frac{5}{16}\right)$, a large compression of 35% along **c** and small decompressions (2%) along **a** and **b**.

Natural graphite, as well as synthetic samples, may contain up to 30% of rhombohedral graphite (RG) in combination with HG. Although RG is considered as an unstable allotrope of carbon, or an extended stacking fault of HG, it has been often involved in the transformation mechanisms between carbon polymorphs [9, 11, 14]. The HG → RG transition mechanism, shown in figures 2(a) → (b) → (c), consists of a reduction of α from 90° in HG to 78.040° in RG, and of fractional displacements of the atoms by $\pm\frac{1}{12}$**b** (figure 2(b)). The hexagonal RG unit cell is deduced from the monoclinic unit cell by shifting the origin by $p = (0, 1/2, 0)$.

The HD and CD structures can be obtained from RG as shown in figures 2(c) → (f) → (i) and 2(c) → (d) → (j), respectively. The RG → HD transition requires an increase of α from 78.040° to 90° and antiparallel displacements (figure 2(g)) by $\pm\frac{1}{48}$**b** and $\pm\frac{1}{12}$**c**. It yields the HD unit cell (figure 2(j)), which requires compressions along **c** (36%) and **b** (3%) and decompression along **a** (3%). The RG → CD transition follows a similar scheme, with a reduction of α from 78.040° to 70.529° and displacements (figure 2(f)) by $\pm\frac{1}{24}$**c** fractions, with a compression along **c** (36%) and decompressions (3%) along **a** and **b**.

2.2. Silicon and germanium

The $Fd\bar{3}m \rightarrow I4_1/amd$ diamond-type-to-β-Sn type transition mechanism, which takes place at 11.7 GPa in Si and at 10.6 GPa in Ge, is shown in figure 3. It involves a stretching of the diamond unit cell along [100] and [010] and a strong compression along [001], which brings the atoms from positions 8a to 4a, with an increase of the coordination number from four to six. The distortions, which are deduced from the lattice parameter values at ambient pressure and at 12–13 GPa [15, 16], are consistent with the observed volume drops, which are 23.7% for Si [17] and 18.4% in Ge [18].

The displacive mechanism associated with the (SiII, GeII) → (SiXI, GeIV) transition ($I4_1/amd \rightarrow Imma$), shown in figure 4(a), consists of antiparallel displacements along the c-axis by about $\pm 0.068c$, the atoms being shifted from positions 4a to 4e without change of the coordination number. Comparison of the lattice parameters in the two phases reveals a small volume change of 0.2% in accordance with the slightly first-order character reported for the transition. The SiXI and GeIV structures can also be deduced by a simple shear deformation from the diamond structure. The orientational relationship between the (SiXI, GeIV) and (SiV, GeV) structures is shown in figure 4(b). The antiparallel displacements of about $\pm 0.057c$ leading to the hexagonal structure ($P6/mmm$) of (SiV, GeV) take place along the [001] orthorhombic direction, bringing the atoms into the onefold position 1a. The compressions

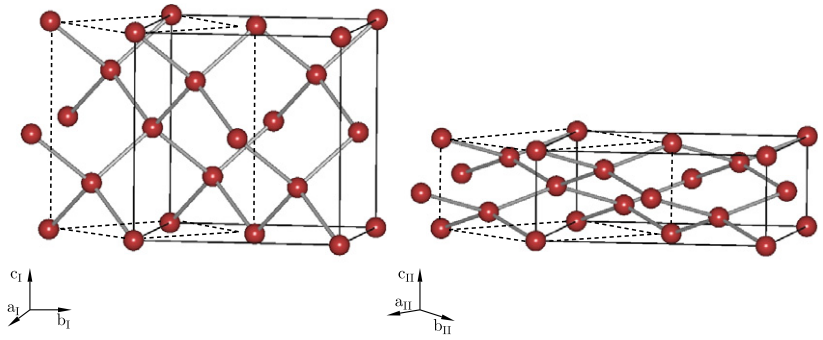

Figure 3. Mechanism transforming the diamond-type structure (left) into the β-Sn-type structure (right) via a stretching of the cubic unit cell along [100] and [010], and a drastic compression along [001]. The orientations of the conventional cells are indicated below the structures.

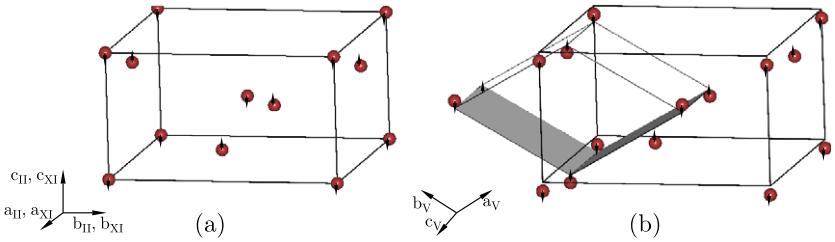

Figure 4. Displacive mechanism associated with the $I4_1/amd \rightarrow Imma \rightarrow P6/mmm$ transitions. The arrows reflect the real magnitude of the atomic displacements. (a) Displacements along [001] transforming the tetragonal (SiII, GeII) structure into the orthorhombic structure of (SiXI, GeIV). For comparison the origin of the orthorhombic cell is shifted to $p = (0, \bar{\frac{1}{4}}, \bar{\frac{1}{8}})$. (b) Orientational relationship between the orthorhombic and hexagonal unit cells and displacements along [001] giving rise to the (SiV, GeV) structure. The origin of the hexagonal cell is shifted to $p = (\bar{\frac{1}{8}}, \bar{\frac{1}{8}}, 0)$.

calculated from the lattice parameters are negligibly small, in agreement with the small volume change of 0.5% reported experimentally [19, 20].

Figure 5 shows the complex set of displacements transforming the preceding hexagonal structure into the orthorhombic structure ($Cmca$) of (SiVII, GeVII). It involves four successive hexagonal layers, denoted 1–4, projected along [100] and [001] in figures 5(a) and (b). The atoms of layers 1 and 3 are displaced in the b/c plane whereas the atoms of layers 2 and 4 are displaced along **a**. Figures 5(c) and (d) represent projections of the resulting orthorhombic structure, which can be described as a four-layer sequence of flat layers of diatomic units, in which layers 1 and 3 are formed by atoms in Wyckoff position 8f and coordination number 11, alternating with buckled square layers 2 and 4 formed by atoms in position 8d and coordination number 10 [21, 22]. The further displacive mechanism transforming SiVI and GeVI into an hcp structure is described in figure 6(a). The atoms pertaining to layers 1 and 3 are shifted parallel to the orthorhombic b/c-plane, whereas the displacement vector for the atoms of layers 2 and 4 has an additional small component along **a**, which transforms the buckled layers 2 and 4 (see figure 5(d)) into the flat layers characteristic for the hexagonal close-packed structure.

Figure 7 shows our proposed displacive mechanism for the Si VII $\rightarrow$ Si X reconstructive transition [23]. Figures 7(a) and (b) represent the hcp and fcc structures with two close-packed layers stacked along $[001]_{\mathrm{hcp}}$ and three close-packed layers stacked along $[111]_{\mathrm{fcc}}$, respectively.

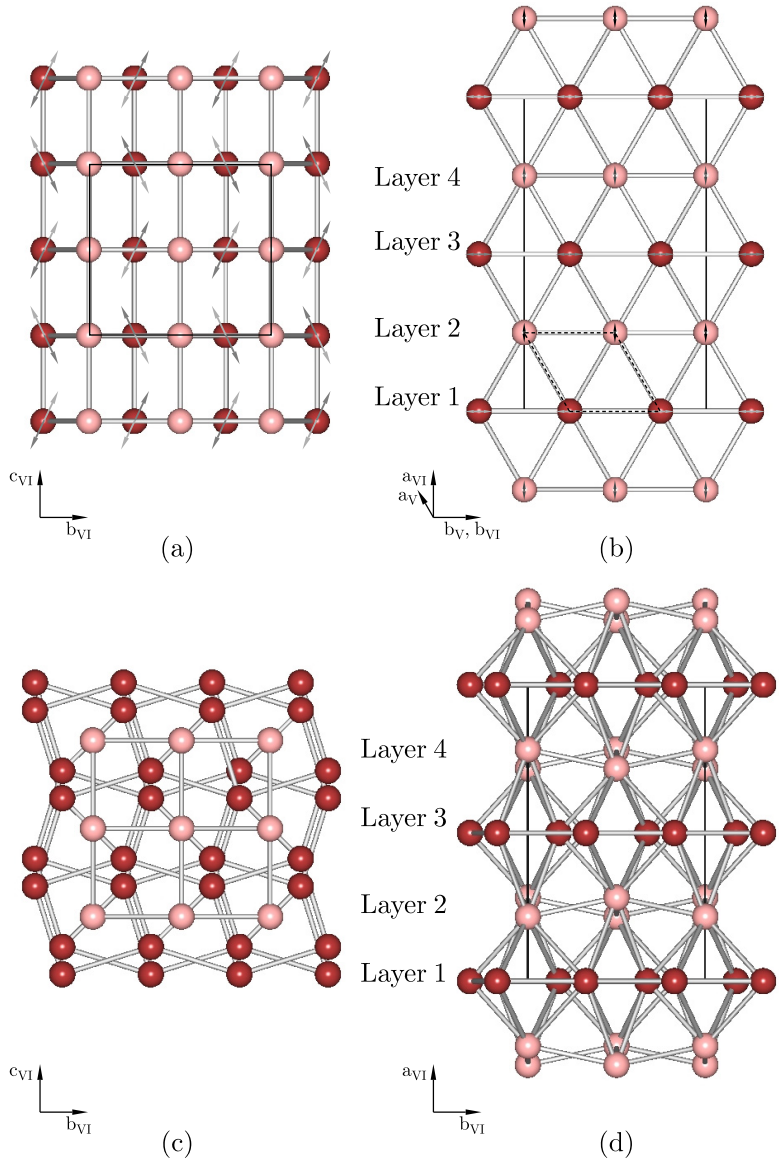

Figure 5. Displacive mechanism associated with the $P6/mmm \rightarrow Cmca$ transition shown in projection along [100] in (a), and along [001] in (b). The unit cell of the hexagonal (SiV, GeV) structure is indicated by broken lines. The origin of the transformed orthorhombic unit cell of (SiV, GeV), represented by solid lines, is shifted to $p = (0, \frac{1}{4}, 0)$. Atoms belonging to different layers stacked along [100] are shown in different grey shades (colours). Their displacements represented by arrows with real magnitudes are in the (100) plane for layers 1 (light grey arrows) and 3 (grey arrows), and along [100] for layers 2 (black arrows) and 4 (dark grey arrows). (c), (d) The resulting (SiVI, GeVI) structure projected along [100] and [001], respectively.

Their common substructure corresponds to an orthorhombic (for hcp) or monoclinic (for fcc) unit cell, shown in the figures, formed by two close-packed layers. Starting from the hcp structure of SiVII the mechanism leading to SiX consists of (1) a shearing strain e_{yz}

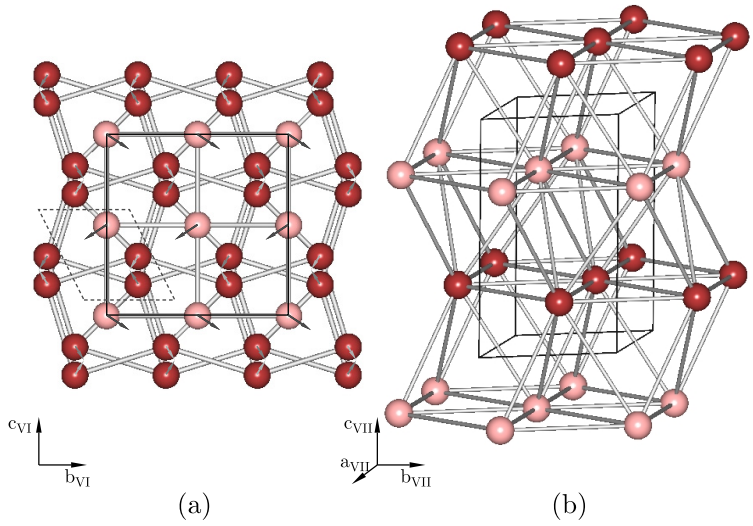

Figure 6. (a) Displacive mechanism associated with the $Cmca \rightarrow P6_3/mmc$ transition. The orthorhombic structure of (SiVI, GeVI) is projected along [100]; the unit cell is indicated by solid lines. The hexagonal unit cell of (SiVII, GeVII) is shown in broken lines with its origin shifted to $p = (\frac{\bar{1}}{8}, \frac{1}{8}, \frac{\bar{1}}{12})$ with respect to the orthorhombic cell. The displacements of the four layers are indicated by light grey arrows (layer 1), black arrows (layer 2), grey arrows (layer 3) and dark grey arrows (layer 4). The resulting hcp structure of (SiVII, GeVII) is represented in (b).

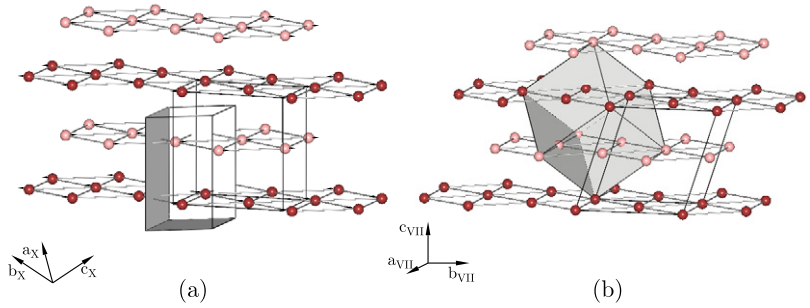

Figure 7. Structural mechanism transforming the hcp structure (a) into the fcc structure of SiX (b). In (a) and (b) the unit cells of the common close-packed bilayer substructure, which has the $Cmcm$ (for hcp) or $C2/m$ (for fcc) symmetry, are represented, together with the conventional hcp and fcc unit cells (grey polyhedra). In (a) the origin of the $Cmcm$ unit cell is shifted to $p = (0, \frac{1}{4}, \frac{1}{4})$. The transition mechanism consists of a shear strain reducing the angle α from 90° to 70.529° and of antiparallel displacements along $[120]_{\mathrm{hcp}}$ shown by arrows of the real magnitude.

reducing the angle α of the orthorhombic ($Cmcm$) subcell from 90° to 70.529° and (2) a set of antiparallel fractional displacements by $\pm\frac{1}{12}$ along $[120]_{\mathrm{hcp}}$, which yields the monoclinic substructure of symmetry $C2/m$ with two layers stacked along **c**, underlying the fcc structure.

In addition to the preceding structural sequences, a number of other structures of Si and Ge have been disclosed. Slow decompression from SiII leads first to the rhombohedral SiXII phase [24] (space group $R\bar{3}$) at about 10 GPa, which transforms reversibly to the body-centred cubic SiIII phase [25] ($Ia\bar{3}$) at about 2 GPa. Moderate heating of SiIII above 400 K yields the hexagonal diamond structure of SiIV ($P6_3/mmc$) [26]. Other metastable structures (labelled VIII and IX) have also been reported on releasing pressure from SiII [27], but their structures

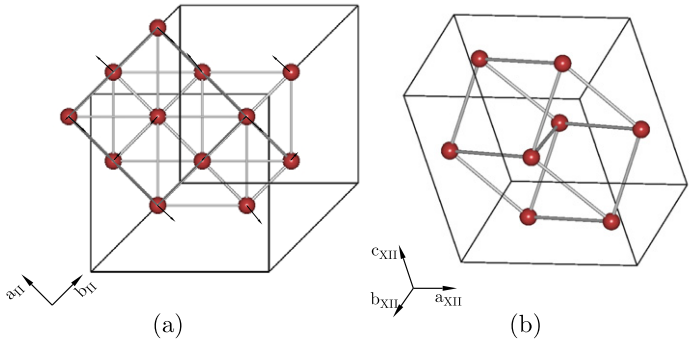

Figure 8. (a) Structure of SiII, projected along [001]. The atomic displacements transforming SiII into SiXII are indicated by arrows. The unit cell of SiII is shown by grey lines. The origin of the transformed unit cell of SiXII, shown in black, is shifted to $p = (\frac{3}{16}, \frac{1}{8}, \frac{3}{16})$. (b) Rhombohedral structure of the metastable SiXII phase.

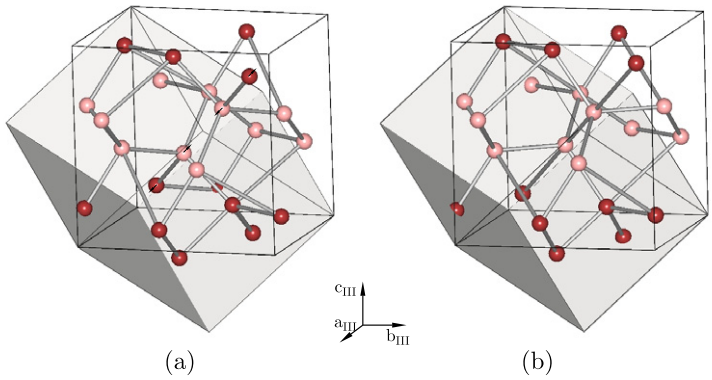

Figure 9. (a) Displacements (arrows) along [111] of the Si atoms transforming the rhombohedral unit cell of SiXII, shown as a grey polyhedron, into the cubic SiIII unit cell (solid lines). (b) Cubic bc8 structure of SiIII.

are unresolved. By decompression of GeII two different phases were found: the GeVIII phase, which has the $Ia\bar{3}$ SiIII structure [28], and the tetragonal GeIII phase ($P4_32_12$) [29]. We were unable to find a consistent transformation path for the GeII $\rightarrow$ GeIII reconstructive transition. The displacive mechanisms leading to SiXII, (SiIII, GeVIII) and SiIV are now described.

Figure 8(a) shows the β-Sn-type structure of SiII projected along [001] and the antiparallel atomic displacements giving rise to the rhombohedral structure of SiXII, shifting the atoms from the 4a positions to the fourfold coordinated positions 2c and 6f. The transition is strongly reconstructive, as expressed by the large volume change occurring at the transition. There exists no direct symmetry relationship between the SiII and SiXII structures. In contrast, the SiXII structure is group–subgroup related to the SiI diamond-type structure and also to the lower-pressure SiIII structure, in which the atoms occupy the 16c positions with a fourfold coordination. SiXII can be deduced from SiIII by a shearing mechanism associated with the spontaneous strain $e_{xy} = e_{yz} = e_{xz}$. The displacements corresponding to the reverse $Ia\bar{3} \rightarrow R\bar{3}$ structural change are shown in figures 9(a) and (b). They take place along the [111] cubic direction. Although SiIII has a diamond related structure, as shown in figure 10, its symmetry has no direct connection with the diamond symmetry, the relationship between the

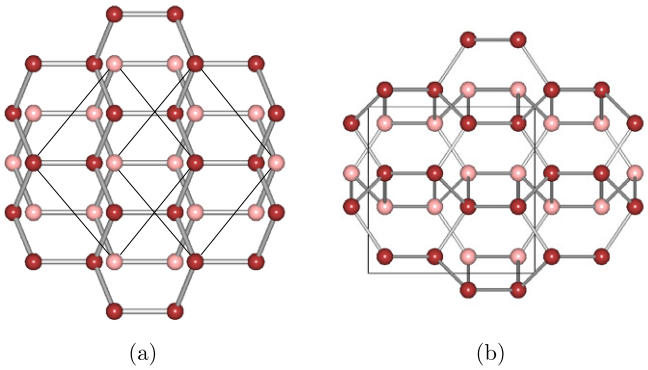

Figure 10. (a) Diamond-type structure of SiI, projected along [112]. (b) Diamond-related character of the SiIII structure shown in projection along [001]. Atoms at different heights along [112] in (a) and [001] in (b) are represented by different grey shades (colours).

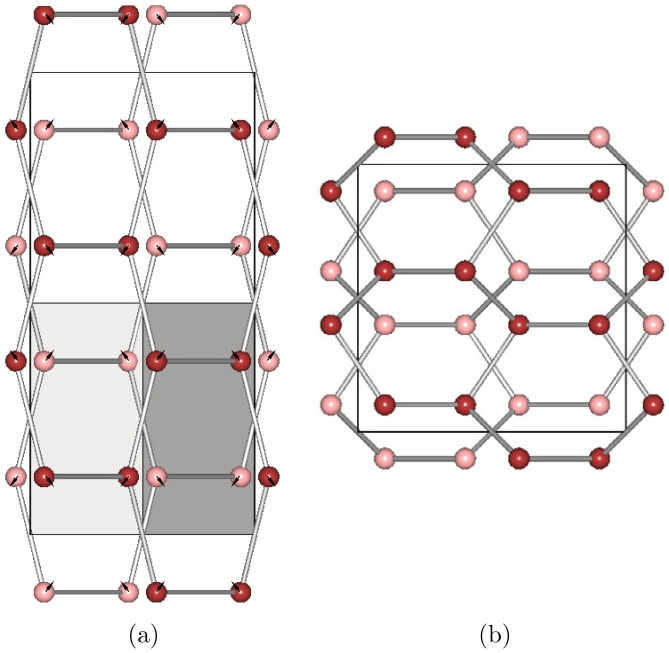

Figure 11. (a) Structure of GeII, projected along [101]. The origin of the transformed unit cell is shifted to $p = (\frac{1}{16}, \frac{1}{8}, \frac{1}{16})$. The arrows indicate the atomic displacements required for a direct transition to the cubic GeVIII structure shown in (b) in projection along [001]. Atoms at different heights along [101] in (a) and [001] in (b) are shown in different grey shades (colours).

two structures occurring via the rhombohedral SiXII structure. This latter structure has not been observed in germanium, where the GeII $\rightarrow$ GeVIII mechanism takes place directly. Figure 11 shows the displacement field which transforms GeII into GeVIII. The strongly reconstructive character of the transition is attested by the large volume change observed at the transition. The transition mechanism from cubic SiIII-to-lonsdaleite-type structure of SiIV [26] is shown in figure 12. It involves small displacements of the atoms within the a/b plane of the cubic SiIII

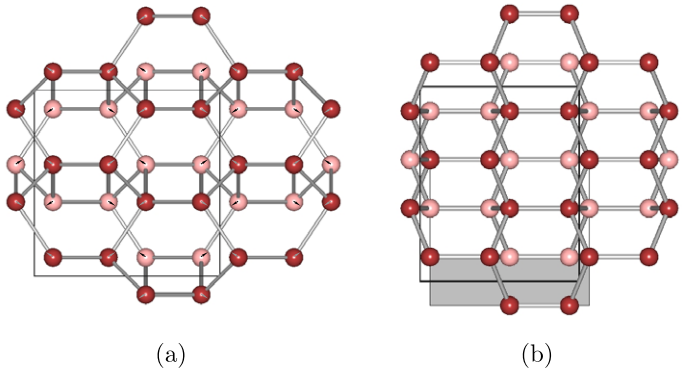

Figure 12. (a) Displacements (arrows of real magnitude) transforming the SiIII structure, projected along [001], into the lonsdaleite-type structure of SiIV, shown in (b) in projection along [120]. In both figures atoms at different heights along [001] in (a) and [120] in (b) are represented in different grey shades (colours). In (b) the origin of the SiIII-related orthorhombic unit cell of SiIV is shifted to $p = (\frac{\bar{1}}{16}, \frac{\bar{1}}{8}, \frac{1}{4})$. The conventional hexagonal unit cell is shown as a grey polyhedron.

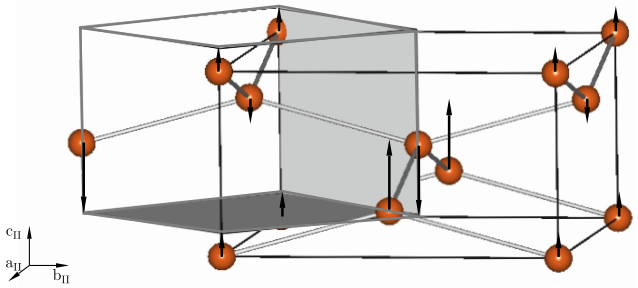

Figure 13. Displacive mechanism associated with the SnI → SnIII → SnIV transitions. The SnI structure (unit cell in black lines) is transformed into the SnIII structure (unit cell in grey lines) by two types of displacement of unequal magnitudes (arrows) along [001]. The tetragonal SnIII to bcc SnIV transition corresponds to a small tensile deformation (see text and table 2) of the grey unit cell. The origins of the tetragonal unit cell of SnIII and the cubic unit cell of SnIV are shifted to $p = (0, 0, \frac{\bar{1}}{8})$.

structure and larger antiparallel displacements of half of the atoms along **c**, bringing the atoms into the 12-fold coordinated positions 2a and 2d.

2.3. Tin

The cubic-diamond-type-to-β-tin SnII → SnI transition takes place both under pressure (0.9 GPa at 78 K) [30] and with increasing temperature (287 K at ambient pressure). Its mechanism is shown in figure 3. Above the β-tin phase two additional transitions occur at about 9.2 and 40 GPa with the structural sequence $I4_1/amd \rightarrow I4/mmm \rightarrow Im\bar{3}m$. The β-Sn-to-simple tetragonal SnI–SnIII transition [31] is shown in figure 13. Two pairs of atoms pertaining to the conventional β-Sn unit cells are shifted by different amounts, $\pm\frac{1}{8}\mathbf{c}$ and $\pm\frac{3}{8}\mathbf{c}$, to the eightfold coordinated position $2a$. The higher-pressure SnIII → SnIV transition [32] corresponds to a simple deformation of the tetragonal unit cell associated with the spontaneous strain $2e_{zz} - e_{xx} - e_{yy}$.

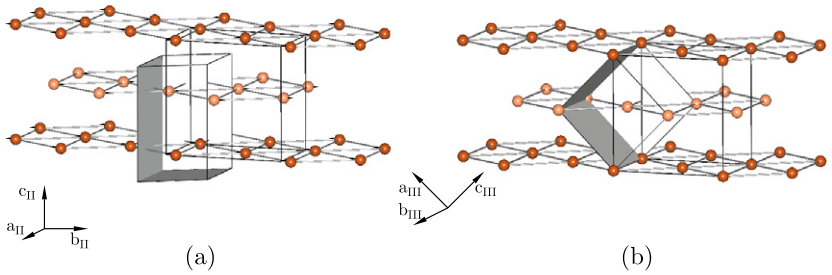

Figure 14. Reverse hcp → bcc Burgers mechanism for the PbII → PbIII transition. The unit cells of the orthorhombic substructure (solid lines) common to the hcp and bcc structures are represented together with the conventional hcp (a) and bcc (b) unit cells, shown as grey polyhedra. In (a) the origin of the orthorhombic unit cell is shifted to $p = (0, \frac{1}{4}, \frac{1}{4})$. The mechanism consists of antiparallel displacements of adjacent (001) layers along $[120]_{\mathrm{hcp}}$ (arrows in (a)) and a tensile deformation (see the text and table 2).

2.4. Lead

The fcc → hcp transition occurring in lead at 13.7 GPa between the PbI and PbII phases [33] follows a reverse path with respect to the mechanism, described in figure 7 for SiVII → SiX. The angle α of the monoclinic two-layered subcell of the fcc structure increases from 70.529° to 90° and additional atomic displacements of $\pm\frac{1}{24}$ along the $[\bar{1}\bar{1}2]_{\mathrm{fcc}}$ direction lead to the hcp structure. The PbII → PbIII hcp-to-bcc transition occurring at 109 GPa [34, 35] corresponds to the reversed Burgers mechanism shown in figure 14. It involves the tensile deformation $e_{xx} - e_{yy}$, which lowers the hcp symmetry to orthorhombic $Cmcm$, and antiparallel displacements of adjacent (001) layers by $\pm\frac{1}{12}[120]_{\mathrm{hcp}}$, which yield the bcc structure.

3. Landau symmetry analysis

3.1. Carbon

In terms of a Landau symmetry analysis the order parameters associated with the transition from HG to the other carbon polymorphs are of two types. (1) Macroscopic strains, which consist of the shear strain e_{yz}, which expresses the changes in the angle α reducing the hexagonal HG symmetry to monoclinic, and the tensile strain $e_{xx} - e_{yy}$, corresponding to an orthorhombic deformation of the hexagonal cell. The additional non-symmetry-breaking component e_{zz} accounts for the compression along **c**. (2) A cooperative set of fractional symmetry displacements along **b** and **c**. Both types of order parameter are activated for obtaining the polymorphic structures which appear as *limit states* arising for definite critical displacements and critical strains. This is consistent with the theoretical approach proposed for reconstructive transitions of the displacive type [36, 37], in which the critical displacements coincide with extrema of the effective order parameters defined as periodic functions of the displacements. The periodic character of the reconstructive transition mechanisms is shown in figure 15, in which the order parameter η is plotted as a function of the atomic displacements ξ along the [120] direction in HG. The periodic function $\eta(\xi)$ representing the effective order parameter associated with the HG → (HD, CD, RG) transitions is the truncated Fourier series:

$$\eta(\xi) = 0.958\sin(6\pi\xi) + 0.125\sin(42\pi\xi). \tag{2}$$

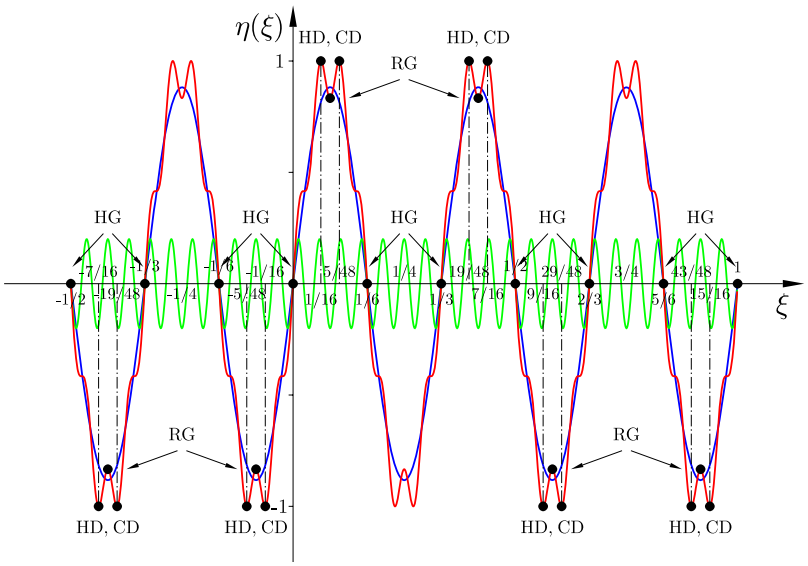

Figure 15. Periodic dependence (grey (red) curve) of the effective transition order parameter $\eta(\xi)$, defined by (2), associated with the transitions from hexagonal graphite (HG) to rhombohedral graphite (RG) and cubic (CD) and hexagonal (HD) diamonds, as a function of the displacements ξ along $[120]_{\mathrm{HG}}$. The curve in black (blue) represents the periodicity of the displacements giving rise to the RG structure (first term in (2)). The light grey (green) curve is a higher harmonic (second term in (2)) whose periodicity reflects the onset of the HD and CD structures from HG and RG, respectively.

The first term in equation (2) expresses the primary symmetry-breaking displacements giving rise to the RG structure from HG, and the second term is a higher harmonic related to secondary symmetry-breaking displacements leading to the HD and CD structures from HG and RG, respectively. Taking into account the transformation properties of the displacements ξ by the symmetry operations of the HG space group ($P6_3/mmc$) yields two distinct effective free energies:

$$F_1(\eta(\xi)) = \frac{\alpha}{2}\eta^2 + \frac{\beta}{4}\eta^4 + \frac{\gamma}{6}\eta^6 \tag{3}$$

for the HG $\rightarrow$ (RG, HD) transitions, and

$$F_2(\eta(\xi)) = \frac{\alpha'}{2}\eta^2 + \frac{\beta'}{3}\eta^3 + \frac{\gamma'}{4}\eta^4 \tag{4}$$

for the HG $\rightarrow$ CD transition. Minimization of F_1 and F_2 with respect to ξ provides the critical displacements ξ^{c} at which the RG, HD and CD phases arise. Their fractional character can be viewed by decomposing ξ^{c} into the critical displacements ξ_1^{c}, along $[120]_{\mathrm{HG}}$, and ξ_2^{c}, along $[001]_{\mathrm{HG}}$. Minimizing F_1 yields the equation of state,

$$\eta\frac{\partial\eta}{\partial\xi}(\alpha + \beta\eta^2 + \gamma\eta^4) = 0 \tag{5}$$

which gives four possible stable states: (i) the HG phase for $\eta = 0$ corresponding to the successive critical displacements, expressed in **b** units for ξ_1^{c} and **c** units for ξ_2^{c}, $\xi_1^{\mathrm{c}} = \pm(0, \frac{1}{6}, \frac{1}{3}, \frac{1}{2}, \frac{2}{3}, \frac{5}{6}, \ldots)$, $\xi_2^{\mathrm{c}} = 0$; (ii) the HD phase for $\frac{\partial\eta}{\partial\xi} = 0$ and $\xi_2^{\mathrm{c}} = \pm(\frac{1}{16}, \frac{5}{48}, \frac{19}{48}, \frac{7}{16}, \frac{9}{16}, \frac{29}{48}, \frac{43}{48}, \frac{15}{16}, \ldots)$, $\xi_2^{\mathrm{c}} = \pm\frac{1}{12}$; (iii) the RG phase for $\frac{\partial\eta}{\partial\xi} = 0$ and $\xi_1^{\mathrm{c}} = \pm(\frac{1}{12}, \frac{5}{12}, \frac{7}{12}, \frac{11}{12}, \ldots)$, $\xi_2^{\mathrm{c}} = 0$, and (iv) the monoclinic $P2/m$ (HG $\rightarrow$ CD) or $C2/m$ (HG $\rightarrow$

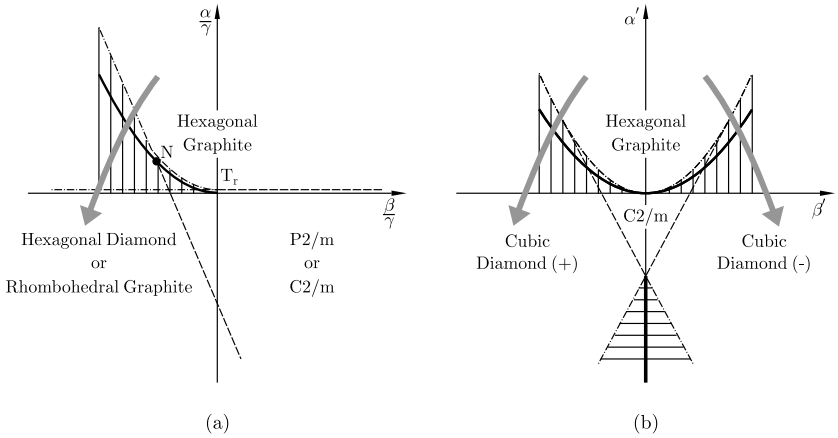

Figure 16. Theoretical phase diagrams corresponding to the minimization of the (a) F_1 and (b) F_2 Landau free energies with respect to the displacements ξ. Solid, dashed and dashed–dotted lines represent, respectively, first-order transition, second-order transition and limit of stability lines. The hatched areas are regions of phase coexistence. N is a three-phase point. T_r is a tricritical point. The arrows suggest the thermodynamic paths followed in carbon.

RG) phases for $\eta = \pm[\frac{1}{2\gamma}(-\beta + \sqrt{\beta^2 - 4\alpha\gamma})]^{1/2}$ and non-critical displacements ξ_1 and ξ_2. Minimization of F_2 with respect to ξ leads to (i) the HG phase for $\eta = 0$; (ii) the CD phase for $\frac{\partial\eta}{\partial\xi} = 0$ and the same critical values of ξ_1^c stabilizing HD but with $\xi_2^c = \pm\frac{1}{16}$ and (iii) the monoclinic $C2/m$ phase for $\eta = \frac{1}{2\gamma'}(-\beta' \pm \sqrt{\beta'^2 - 4\alpha'\gamma'})$ and non-critical displacements.

Theoretical phase diagrams associated with F_1 and F_2 are shown in figures 16(a) and (b). In figure 16(a) the monoclinic phase can be reached from HG and (HD or RG) across second-order transitions, whereas the HG $\rightarrow$ (HD or RG) reconstructive transitions are always first order. The phase diagram of figure 16(b) reveals the existence of two anti-isostructural CD structures (denoted + or −) associated with opposed signs of η.

3.2. Other IVa elements

The results deduced from the analysis of the structural changes taking place in Si, Ge, Sn and Pb, in the framework of the Landau approach, are summarized in table 2. Column (a) of the table lists the space-group changes occurring at the transitions, with the respective number of atoms in the *primitive* unit cells. For each transition columns (b) and (c) give the relationship between the lattice vectors of the *conventional* unit cells and the corresponding volume change. The other columns of the table detail the results of the Landau symmetry analysis, such as (d) irreducible representations (IRs) of the parent space group inducing the symmetry breaking mechanism. The notation of the IRs follows the table of Stokes and Hatch [38], except for $\tau_1(B)$, $\tau_1(R)$ and $\tau_1(\Sigma)$, which refer to the tables of Zak *et al* [39]. (e) Dimension of the IRs and of the corresponding order parameters. (f) Equilibrium relationship for the order-parameter components (η_i), deduced from the minimization of the associated Landau free energies. The (e_{ij}) denote strain-tensor components; (d_{14}, d_{36}) are components of the piezoelectric tensor. (g) Secondary strains associated with the transitions. The last column (h) labels the phases of the elements of group IVa involved in the structural change indicated in column (a). Figures 17 and 18 show the thermodynamic paths relating the different phases observed in Si, Ge, Sn and Pb with increasing or releasing pressure, and the symmetry relationships found between the corresponding structures. It suggests the following remarks.

Table 2. Structural changes and order-parameter symmetries for the transitions occurring between neighbouring phases in Si, Ge, Sn and Pb, on increasing or releasing pressure. Explanations for the different entries are given in the text.

(a)	(b)	(c)	(d)	(e)	(f)	(g)	(h)
$Fd\bar{3}m(2)$ $\rightarrow I4_1/amd(2)$	$\frac{\mathbf{a}-\mathbf{b}}{2}$, $\frac{\mathbf{a}+\mathbf{b}}{2}$, $\mathbf{c}$	$\frac{1}{2}$	Γ_3^+	2	$\eta_1 = 0$, $\eta_2 = 2e_{zz} - e_{xx} - e_{yy}$	e_{zz}	SiI $\rightarrow$ SiII, GeI $\rightarrow$ GeII, SnII $\rightarrow$ SnI
$I4_1/amd(2)$ $\rightarrow Imma(2)$	$\mathbf{a}$, $\mathbf{b}$, $\mathbf{c}$	1	Γ_2^+	1	$\eta = e_{xx} - e_{yy}$	e_{zz}	SiII $\rightarrow$ SiXI, GeII $\rightarrow$ GeIV
$Imma(2)$ $\leftrightarrow P6/mmm(1)$	$\frac{\mathbf{b}+\mathbf{c}}{2}$, $\frac{\mathbf{c}-\mathbf{b}}{2}$, $\frac{\mathbf{a}}{2}$	$\frac{1}{4}$	L_3^-	3	$\eta_1 \neq 0$, $\eta_2 = \eta_3 = 0$	$e_{xx} - e_{yy}$	SiXI $\rightarrow$ SiV, GeIV $\rightarrow$ GeV
$P6/mmm(1)$ $\rightarrow Cmca(8)$	$4\mathbf{a} + 2\mathbf{b}$, $2\mathbf{b}$, $2\mathbf{c}$	16	$\tau_1(B)$	12	$\eta_1 = \eta_2 \neq 0$, $\eta_{3\rightarrow 12} = 0$	$e_{xx} - e_{yy}$	SiV $\rightarrow$ SiVI, GeV $\rightarrow$ GeVI
$Cmca(8)$ $\leftrightarrow P6_3/mmc(2)$	$\frac{\mathbf{b}}{2}$, $\frac{\mathbf{c}}{2} - \frac{\mathbf{b}}{4}$, $\frac{\mathbf{a}}{2}$	$\frac{1}{8}$	$\tau_1(R)$	6	$\eta_1 = \eta_2 \neq 0$, $\eta_{3\rightarrow 6} = 0$	$e_{xx} - e_{yy}$	SiVI $\rightarrow$ SiVII, GeVI $\rightarrow$ GeVII
$P6_3/mmc(2)$ $\rightarrow Fm\bar{3}m(1)$	$-\frac{3}{2}\mathbf{a} - \mathbf{b} + \frac{\mathbf{c}}{2}$, $\frac{\mathbf{a}}{2} - \mathbf{b} + \frac{\mathbf{c}}{2}$, $\frac{\mathbf{a}}{2} + \mathbf{b} + \frac{\mathbf{c}}{2}$	$\frac{1}{2}$	Γ_6^+	2	$e_{yz} \neq 0$, $e_{xz} = 0$	$e_{xx} - e_{yy}$	SiVII $\rightarrow$ SiX
$I4_1/amd(2)$ $\leftrightarrow I4/mmm(1)$	$\frac{\mathbf{a}-\mathbf{b}}{2}$, $\frac{\mathbf{a}+\mathbf{b}}{2}$, $\mathbf{c}$	$\frac{1}{2}$	P_5 $+\Gamma_2^-$	$4+1$	$\eta_1 \neq 0$, $\eta_{2\rightarrow 4} = 0$, (d_{14}, d_{36})	—	SnI $\rightarrow$ SnIII
$I4/mmm(1)$ $\leftrightarrow Im\bar{3}m(1)$	$\mathbf{a}$, $\mathbf{b}$, $\mathbf{c}$	1	Γ_3^+	2	$\eta_1 = 0$, $\eta_2 = 2e_{zz} - e_{xx} - e_{yy}$	e_{zz}	SnIII $\rightarrow$ SnIV
$Fm\bar{3}m(1)$ $\rightarrow P6_3/mmc(2)$	$\frac{\mathbf{b}-\mathbf{a}}{2}$, $\frac{\mathbf{c}-\mathbf{b}}{2}$, $\frac{\mathbf{a}+\mathbf{b}}{2} + \mathbf{c}$	$\frac{1}{2}$	L_3^- $+\Gamma_5^+$	$8+3$	$\eta_1 = \eta_2 \neq 0$, $\eta_{3\rightarrow 8} = 0$, $e_{yz} = -e_{xz}$, e_{xy}	$2e_{zz} - e_{xx}$ $-e_{yy}$	PbI $\rightarrow$ PbII
$P6_3/mmc(2)$ $\leftrightarrow Im\bar{3}m(1)$	$\mathbf{b}$, $\frac{\mathbf{c}-\mathbf{a}-\mathbf{b}}{2}$, $\mathbf{a} + \mathbf{c}$	$\frac{1}{2}$	N_2^- $+\Gamma_5^+$	$6+2$	$\eta_1 \neq 0$, $\eta_{2\rightarrow 6} = 0$, $e_{xy} = 0$, $e_{xx} - e_{yy} \neq 0$	e_{zz}	PbII $\rightarrow$ PbIII
$Fd\bar{3}m(2)$ $\rightarrow R\bar{3}(8)$	$\mathbf{b}$, $\frac{\mathbf{c}-\mathbf{a}-\mathbf{b}}{2}$, $\mathbf{a}$	1	X_2	6	$\eta_1 = \eta_3 = \eta_5 = 0$, $\eta_2 = \eta_4 = \eta_6 \neq 0$	$e_{xy} = e_{xz} = e_{yz}$	SiI $\rightarrow$ SiXII
$R\bar{3}(8)$ $\leftrightarrow Ia\bar{3}(8)$	$\mathbf{b} + \mathbf{c}$, $\mathbf{a} + \mathbf{c}$, $\mathbf{a} + \mathbf{b}$	$\frac{1}{2}$	Γ_4^+	3	$e_{xy} = e_{xz} = e_{yz}$	—	SiXII $\rightarrow$ SiIII
$Ia\bar{3}(8)$ $\leftrightarrow P6_3/mmc(4)$	$\frac{2\mathbf{a}-\mathbf{b}}{4}$, $\frac{\mathbf{b}}{2}$, $\mathbf{c}$	$\frac{1}{4}$	$\tau_1(\Sigma)$ $+H_2^+$	$6+2$	$\eta_1 = \eta_2 \neq 0$, $\eta_{3\rightarrow 6} = 0$ $\xi_1 \neq 0$, $\xi_2 \neq 0$, $e_{xx} - e_{yy}$	$2e_{zz} - e_{xx}$ $-e_{yy}$	SiIII $\rightarrow$ SiIV

(1) The common sequence of phases found in Si and Ge can be interpreted as a series of displacive reconstructive group–subgroup unrelated structural changes $I4_1/amd \rightarrow P6/mmm \rightarrow P6_3/mmc$, the $Imma$ and $Cmca$ phases playing the role of intermediate paths which allow the reconstructive mechanisms to take place in a less abrupt way. These intermediate structures are reminiscent of the parent diamond-type structure to which they are group–subgroup related. The transition to the β-Sn structure, which is adjacent to the parent structure, presents a hybrid character: its mechanism shows reconstructive features, such as the drastic volume compression, and its irreversible character, which leads to the formation of different metastable phases on releasing pressure, but its symmetry remains group–subgroup

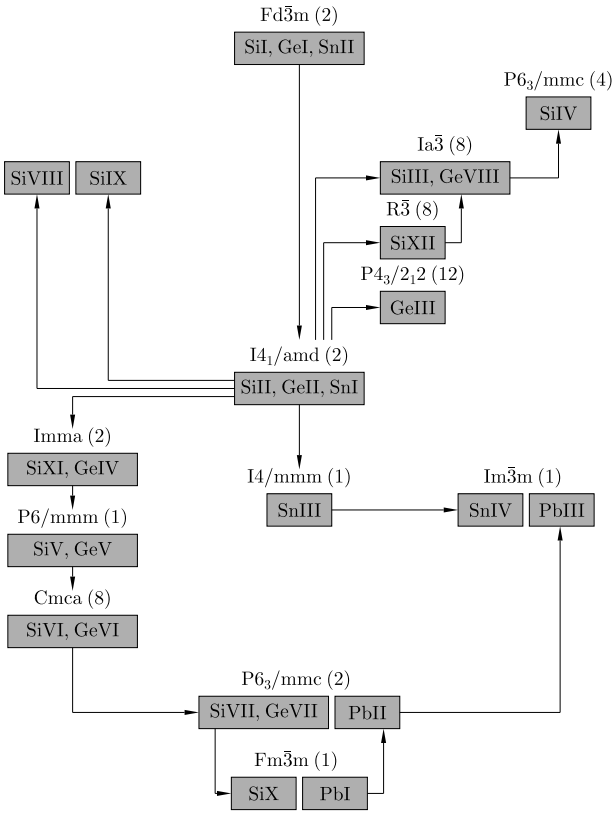

Figure 17. Summary of the different structures disclosed on increasing or releasing pressure in Si, Ge, Sn and Pb. The SiIV phase is obtained on heating SiIII.

related to the diamond structure. The reconstructive structural change $I4_1/amd \rightarrow Ia\bar{3}$, which takes place on releasing pressure, follows the same scheme going across the intermediate $R\bar{3}$ phase, which is closely related to the diamond phase.

The sequences of phases in Si and Ge shows a steady increase in coordination number from 4 in (SiI, GeI) to 12 in (SiVII, GeVII). The occurrence of fourfold coordinated structures at low pressures is usually explained [40] by the formation of strong sp^3 hybridized orbitals on each atom, which are directed from the centre of a cube along the opposite body diagonals. In carbon the absence of a p-electron state in the $1s^2$ atomic core allows the strongly p-character sp^3 bonding electrons in diamond to be held close to the nucleus. At variance, the large variety of chemical bonding situations encountered in Si and Ge with increasing pressure can be related to the balance between a decrease in the tendency to form sp bonds and an increase in the promotion of electrons from the s state to the p state. The evolution between these two tendencies occurs progressively with increasing pressure, the successive formation of allotropes reflecting the simultaneous increasing occupation of p states by the electrons, the corresponding depletion of the s states and the continuous sp dehybridization process. The fact that the intervals of stability of the high-pressure phases are very different, as the result of a considerably larger interval of stability for GeII than for SiII, has been attributed [41] to the effect of d electrons in Ge: the larger and more polarizable core containing the 3d electrons in Ge repels the d-like valence electrons which are created as the originally empty 4d states

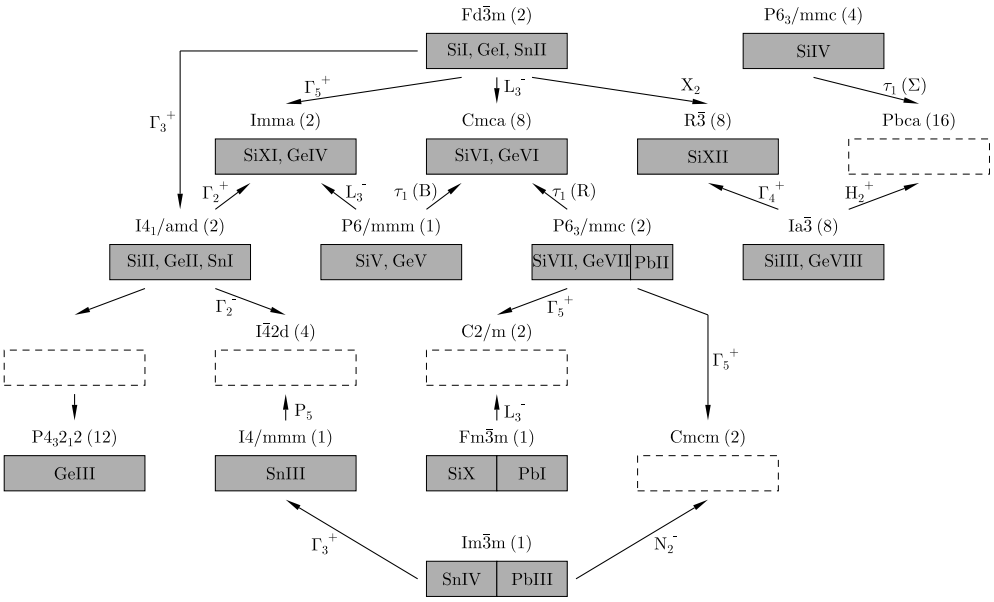

Figure 18. Connections between the different structures of Si, Ge, Sn and Pb, as deduced from a Landau symmetry analysis. The irreducible representations associated with the symmetry-breaking mechanisms are indicated along the arrows relating the structures. The intermediate structures assumed in our proposed transition mechanisms and not observed experimentally are indicated by rectangles in broken lines.

are lowered in pressure. As a consequence, it raises the energies and pressures, leading to the higher transition pressures between metallic phases. In this respect, the fact that the hcp GeVII phase arises at very high pressure (170 GPa) with a ratio c/a close to the ideal value 1.633 [22] does not favour the onset of a higher-pressure closer-packed fcc phase. In contrast, in Si the hcp SiVII phase takes place at the lower pressure of 79.2 GPa, the c/a ratio varying in this phase from 1.70 down to 1.67 [23]. Therefore, the SiX fcc structure represents a closer atomic packing, attested by the continuous decrease of its unit-cell volume up to 248 GPa.

(2) In Sn the complex mechanism taking place at the $I4_1/amd \rightarrow I4/mmm$ reconstructive transition seems to mark the end of the influence of the diamond-type structure, which occupies a much narrower low-pressure and low-temperature region of the phase diagram, as compared to Si and Ge. The change of structural regime at the transition between the two body-centred tetragonal phases supports the interpretation [42] suggesting that tin is at the borderline where the gain in energy obtained by forming sp^3 bonds does not exceed the $s \rightarrow p$ promotion energy costs. Therefore, the SnIII and SnIV structures reflect the domination of p-electron states on sp hybridization. The disappearance of the diamond-type structure in lead confirms this tendency, which is also supported by first-principle calculations [43] showing that relativistic effects, in which the 6s energy drops far below the 6p energy, can explain the preference of Pb for a low-pressure fcc structure over other, diamond-type, hcp or bcc, structures. However, this does not explain why in Pb the less close-packed bcc structure occupies the highest-pressure region of the phase diagram. A possible answer to this question can be found in the observed properties of the fcc $\rightarrow$ hcp [35] and hcp $\rightarrow$ bcc [44] transitions: The very small volume drops at the transitions, which are in contradiction with the strongly reconstructive character assumed for their mechanisms, are accompanied by large hysteresis extending over several gigapascals, i.e. the transitions are smeared out over a large range

of pressure. Their sluggish character is reminiscent of the behaviour observed for the low-temperature martensitic transitions in lithium and sodium [45], which has been related to the softness of their crystalline state, characterized by a large plastic anisotropy and by flow stress versus temperature curves different from those of usual bcc metals. The softness of lead is attested by the large decrease of the lattice parameters from ambient pressure to 120 GPa, its volume reducing continuously by more than 50% in this interval [33]. This can be pictured at the atomic level by assuming an interpenetration of polarizable Pb atoms that would allow a closer bcc packing at the highest pressures. Such a property may also justify the stability of the high-pressure bcc structure in tin.

4. Summary and discussion

In summary, the different neighbouring structures observed under pressure in the elements of group IVa have been related by displacive transition mechanisms. Two situations have been distinguished. (1) In carbon, starting from the HG structure the carbon allotropes appear as limit states stabilizing for definite critical displacements and critical strains. This interpretation has been justified by expressing the effective transition order parameters as periodic functions of the displacements, the critical displacements corresponding to minima of the free energies and to extrema of the order parameters. The description of the formation of the carbon polymorphs in terms of displacive processes is in contrast with the current interpretations which assume *ordering* mechanisms [9, 11]. Ordering processes are suggested by the possibility of organizing the carbon structures as different stackings of hexagonal layers and the transitions between them as a reordering in the layer stacking. Combined ordering and compression mechanisms allow one to describe the HG $\rightarrow$ CD or the HG $\rightarrow$ RG transitions, but fail to explain the formation of HD because of its orientational relationship with respect to HG. The different orientations of the hexagonal layers reported in cubic and hexagonal diamond, with respect to HG, are essential in favour of a displacive mechanism. The fact that similar critical displacements, involving the same intermediate substructure, yield the variety of carbon polymorphs is another argument in favour of our proposed displacive approach. This approach suggests an explanation of the simplicity of the equilibrium phase diagram of carbon, which contains only the HG and CD phases, as compared to the rich polymorphism found in the phase diagrams of Si, Ge and Sn. Starting from the ambient pressure HG phase, the thermodynamic path assumed for the HG $\rightarrow$ CD transition differs from the paths leading to HD or RG, a further transition from CD to another structure being unlikely due to the limit character of the CD structure, which makes it less sensitive to the influence of temperature and pressure. The left- or right-hand side of the theoretical phase diagram of figure 16(b), which exhibits only the HG and CD phases, reflects the topology of the experimental phase diagram of carbon. The anti-isostructural CD variant may coincide with the cubic n-diamond structure, obtained by rapid cooling from graphite sheet shock-compressed to 65 GPa, which is composed of hexagonal-ring planes puckered in the opposite direction with respect to CD. This is consistent with the opposite signs of the corresponding order parameters.

(2) The absence of the graphite structure in Si and Ge creates the possibility for the diamond-type structure to influence the polymorphism observed at high pressure in these elements. The symmetry analysis of their transition mechanisms reveals indeed that the orthorhombic structures can be directly derived from the diamond-type structure. These low-symmetry structures are intermediate steps in the sequence of reconstructive transitions found in Si and Ge. The influence of the diamond structure, which also shows on the diamond-related lonsdaleite structure of SiIV, is interrupted in Sn by the SnI–SnIII transition, which terminates the series of structures in which the chemical bonds are mainly determined by sp

hybridization, starting the onset of bcc-based structures at higher pressure, with new types of bonding dominated by p-electron states. This tendency is confirmed in Pb, whose sequence of reconstructive transitions displays unusual features which may be attributed to the specific polarizability of the Pb atoms.

With the exception of the classical grey-to-white tin transition, which follows a strain induced ferroelastic mechanism, there has been, to our knowledge, no attempt to describe theoretically the displacive mechanisms relating the different structures involved in the elements of group IVa. Most of the theoretical studies on these elements have been devoted to justifying or to predicting the existence of new high-pressure structures and their electronic properties (see [4] for a review). In the present work we have attempted to give a comprehensive picture of the transformation paths in terms of displacement fields. From purely symmetry or geometrical considerations a number of different transition paths could be *a priori* proposed, relating the various structures. However, when taking into account the real atomic positions, the actual orientational relationship between neighbouring structures, the shortest set of displacements relating the initial and final atomic positions (assuming implicitly a minimal energy principle for the real transformation) and, last but not least, the overall consistency of the successive mechanisms in a given element, then the possible transformation paths were found to be, in most cases, unique.

References

[1] Young D A 1991 *Phase Diagrams of the Elements* (Berkeley, CA: University of California Press)
[2] Nelmes R J and McMahon M I 1998 *Semicond. Semimet.* **54** 145
[3] Tonkov E Yu and Poniatovsky E G 2005 *Phase Transformations of Elements under High Pressure* (Boca Raton, FL: CRC Press)
[4] Mujica A, Rubio A, Munoz A and Needs R J 2003 *Rev. Mod. Phys.* **75** 863
[5] Lipson H and Stokes A R 1942 *Proc. R. Soc.* A **181** 101
[6] Davies G and Evans T 1972 *Proc. R. Soc.* A **328** 413
[7] Fahy S, Louie S G and Cohen M I 1987 *Phys. Rev.* B **35** 7623
[8] Fahy S and Louie S G 1987 *Phys. Rev.* B **36** 3373
[9] Dmitriev V P, Rochal S B, Gufan Yu M and Tolédano P 1989 *Phys. Rev. Lett.* **62** 2495
[10] Scandolo S, Bernasconi M, Chirotti G L, Focher P and Tosatti E 1995 *Phys. Rev. Lett.* **74** 4015
[11] Sung J 2000 *J. Mater. Sci.* **35** 6041
[12] Ghiringhelli L M, Los J H, Meijer E J, Fasolino A and Frenkel D 2005 *Phys. Rev. Lett.* **94** 145701
[13] Bundy F P and Kasper J S 1967 *J. Chem. Phys.* **46** 3437
[14] Fahy S, Louie S G and Cohen M L 1986 *Phys. Rev.* B **34** 1191
[15] Bundy F P 1964 *J. Chem. Phys.* **41** 3809
[16] Soma T and Matsuo H 1982 *J. Phys. C: Solid State Phys.* **15** 1873
[17] Goto T, Sato T and Syono Y 1982 *Japan. J. Appl. Phys.* 2 **21** L369
[18] Menoni C C, Hu J Z and Spain I L 1986 *Phys. Rev.* B **34** 362
[19] McMahon M I, Nelmes R J, Wright N G and Allan D R 1994 *Phys. Rev.* B **50** 739
[20] Vohra Y K, Brister K E, Desgreniers S, Ruoff A L, Chang K J and Cohen M L 1986 *Phys. Rev. Lett.* **56** 1944
[21] Hanfland M, Schwarz U, Syassen K and Takemura K 1999 *Phys. Rev. Lett.* **82** 1197
[22] Takemura K, Schwarz U, Syassen K, Hanfland M, Christensen N E, Novikov D L and Loa I 2000 *Phys. Rev.* B **62** R10603
[23] Duclos S J, Vohra Y K and Ruoff A L 1990 *Phys. Rev.* B **41** 12021
[24] Crain J, Ackland G J, Maclean J R, Piltz R O, Hatton P D and Pawley G S 1994 *Phys. Rev.* B **50** R13043
[25] Piltz R O, Maclean J, Clark S J, Ackland G J, Hatton P D and Crain J 1995 *Phys. Rev.* B **52** 4702
[26] Besson J M, Mokhtari E H, Gonzalez J and Weill G 1987 *Phys. Rev. Lett.* **59** 473
[27] Zhao Y X, Buehler F, Sites J R and Spain I L 1986 *Solid State Commun.* **59** 679
[28] Nelmes R J, McMahon M I, Wright N G, Allan D R and Loveday J S 1993 *Phys. Rev.* B **48** R9883
[29] Kasper J S and Richards S M 1964 *Acta Crystallogr.* **17** 752
[30] Stager R A, Balchan A S and Drickamer H G 1962 *J. Chem. Phys.* **37** 1154
[31] Olijnyk H and Holzapfel W B 1984 *J. Physique Coll.* **45** (Suppl. 11) C8 153

[32] Liu L G and Bassett W 1986 *Elements, Oxides, Silicates* (New York: Oxford University Press)
[33] Desgreniers S, Vohra Y K and Ruoff A L 1989 *Phys. Rev.* B **39** 10359
[34] Mao H K, Wu Y, Shu J F, Hu J Z, Hemley R J and Cox D E 1990 *Solid State Commun.* **74** 1027
[35] Vanderborgh C A, Vohra Y K, Xia H and Ruoff A L 1990 *Phys. Rev.* B **41** 7338
[36] Dmitriev V P, Rochal S B, Gufan Yu M and Tolédano P 1988 *Phys. Rev. Lett.* **60** 1985
[37] Tolédano P and Dmitriev V 1996 *Reconstructive Phase Transitions* (Singapore: World Scientific)
[38] Stokes H T and Hatch D M 1988 *Isotropy Subgroups of the 230 Crystallographic Space Groups* (Singapore: World Scientific)
[39] Zak J, Cacher A, Glück H and Gur Y 1969 *Irreducible Representations of Space Groups* (New York: Benjamin)
[40] Yin M T and Cohen M L 1983 *Phys. Rev. Lett.* **50** 2006
[41] Chang K J and Cohen M L 1986 *Phys. Rev.* B **34** 8581
[42] Christensen N E and Methfessel M 1993 *Phys. Rev.* B **48** 5797
[43] Christensen N E, Sapathy S and Pawlowska Z 1986 *Phys. Rev.* B **34** 5977
[44] Liu A Y, Garcia A, Cohen M L, Godwal B K and Jeanloz R 1991 *Phys. Rev.* B **43** 1795
[45] Blaschko O, Dmitriev V, Krexner G and Tolédano P 1999 *Phys. Rev.* B **59** 9095